



Published in final edited form as:

Neuron. 2016 July 6; 91(1): 133–145. doi:10.1016/j.neuron.2016.05.019.

Mechanism of high frequency signaling at a depressing ribbon synapse

Chad P. Grabner¹, Charles P. Ratliff², Adam C. Light³, and Steven H. DeVries^{*}

Departments of Ophthalmology & Physiology, Northwestern University Feinberg School of Medicine, Chicago, IL 60611, USA

SUMMARY

Ribbon synapses mediate continuous release in neurons that have graded voltage responses. While mammalian retinas can signal visual flicker at 80-100 Hz, the time constant, τ , for refilling of a depleted vesicle release pool at cone photoreceptor ribbons is 0.7–1.1 s. Due to this prolonged depression, the mechanism for encoding high temporal frequencies is unclear. To determine the mechanism of high frequency signaling, we focused on an Off cone bipolar cell type in the ground squirrel, the cb2, whose transient postsynaptic responses recovered following presynaptic depletion with a τ of ~ 0.1 s, or 7-10-fold faster than the τ for presynaptic pool refilling. The difference in recovery time course is caused by AMPA receptor saturation, where partial refilling of the presynaptic pool is sufficient for a full postsynaptic response. By limiting the dynamic range of the synapse, receptor saturation counteracts ribbon depression to produce rapid recovery and facilitate high frequency signaling.

INTRODUCTION

The dynamic properties of synaptic ribbons convert simple voltage inputs into complex transmitter outputs. During repetitive stimuli, synaptic ribbons cycle between phasic and tonic release (DeVries, 2000; Grabner and Zenisek, 2013; Rabl et al., 2005; Singer and Diamond, 2003). Phasic release occurs when a rapid depolarization synchronously opens voltage-gated Ca^{2+} channels near membrane-docked and primed vesicles (Mennerick and Matthews, 1996). The abrupt rise in intracellular Ca^{2+} triggers a burst of vesicle fusion and glutamate release that causes a large, transient postsynaptic response (von Gersdorff et al., 1998). If the depolarization continues, phasic release tails into tonic or sustained release, which occurs at slower rates than phasic release because new vesicles have to translocate to

^{*}Corresponding author; Contact: Steven H. DeVries, MD, PhD, Departments of Ophthalmology & Physiology, Northwestern University Feinberg School of Medicine, Chicago, IL 60611, USA, s-devries@northwestern.edu.

¹Current address is Max Planck Institute for Biophysical Chemistry, Am Fassberg 11, 37077 Göttingen, Germany;

²Current address is Jules Stein Eye Institute, Dept of Ophthalmology, University of California, Los Angeles, CA 90095, USA;

³Current address is WaveMetrics, Inc., Lake Oswego, OR 97035, USA

Publisher's Disclaimer: This is a PDF file of an unedited manuscript that has been accepted for publication. As a service to our customers we are providing this early version of the manuscript. The manuscript will undergo copyediting, typesetting, and review of the resulting proof before it is published in its final citable form. Please note that during the production process errors may be discovered which could affect the content, and all legal disclaimers that apply to the journal pertain.

AUTHOR CONTRIBUTIONS Experiments and data analysis, C.P.G, A.C.L., and S.H.D.; modeling, C.P.R.; writing, C.P.G., C.P.R., and S.H.D.

membrane docking sites and undergo priming before Ca^{2+} can trigger fusion (Jackman et al., 2009). Upon membrane hyperpolarization, Ca^{2+} channels close, but vesicle recruitment and priming continues, and leads to a time-dependent replenishment of releasable vesicles, forming the basis for the next phasic episode (DeVries, 2000; Jackman et al., 2009; Singer and Diamond, 2003). The maximal phasic release can be 10–20 fold larger than tonic release during a comparable interval (DeVries and Schwartz, 1999). However, the size of the phasic component and its impact on subsequent signaling is not fixed, but instead depends on a balance between the temporal frequencies that are signaled by a sensory neuron and the replenishment rate at its ribbons. High replenishment rates support transient signaling at high frequencies but incur a metabolic cost.

When depolarized in the dark, cone ribbons mediate glutamate release onto Off bipolar cells that express AMPA/kainate receptors (DeVries, 2000). Mammalian Off bipolar cells can be subdivided into five anatomical types that differ with respect to their morphology (Helmstaedter et al., 2013; Light et al., 2012; Tsukamoto and Omi, 2015) and temporal light responses. At least one type produces a transient membrane depolarization after a light step, whereas other types have more sustained responses (Baden et al., 2013; DeVries et al., 2006; Ichinose and Hellmer, 2015; Pang et al., 2012). The spatiotemporal interplay between responses in transient and sustained bipolar cell types may be critical for directional signaling (Kim et al., 2014) which first emerges in starburst amacrine cells. In addition, transient and sustained bipolar cells may provide input to transient and sustained ganglion cells (Cleland et al., 1971). Against the idea that the cone to Off bipolar cell synapse can be the origin of transient signaling over the temporal range of cone vision (up to 100 Hz) (Derrington and Lennie, 1984; Smith et al., 2001; Jacobs et al., 1980) is the observation that ribbon vesicle docking sites are replenished with τ of 0.7 – 1.5 s (Innocenti and Heidelberger, 2008; Jackman et al., 2009; Rabl et al., 2006), equivalent to a corner frequency of ~0.2 Hz.

Mammalian cone terminals contain 20 – 40 membrane invaginations, unique ultrastructural specializations of unknown function, that are marked at their apex by a synaptic ribbon (Chun et al., 1996; Dowling and Boycott, 1966). In the cone dominant retina of the ground squirrel, AMPA-receptor-expressing Off cb2 bipolar cell dendrites enter invaginations and terminate 0.1 – 0.2 μm from ribbon active zones, while other Off bipolar cell types contact cones at more distant sites (0.4 – 0.8 μm) at the base of the terminal (Figure 1, inset) (DeVries et al., 2006; Hopkins and Boycott, 1997). We hypothesize that invaginating cb2 contacts promote receptor saturation during the near-synchronous release of ribbon membrane-docked vesicles at light-off. Under saturating conditions, the replenishment and release of vesicles from a small fraction of the available docking sites can elicit a large fraction of the postsynaptic response, overcoming depression to speed up the recovery of the synaptic transient, which in turn facilitates high frequency signaling. AMPA receptor saturation has been described at synapses that use action potentials, including the climbing fiber to Purkinje cell synapse (Foster et al., 2002; Harrison and Jahr, 2003; Wadiche and Jahr, 2001) and the calyx of Held (Neher and Sakaba, 2001; Sun and Wu, 2001). At these synapses, saturation promotes high frequency signaling by providing a safety factor that combats fatigue. We show that receptor saturation also promotes high frequency signaling during graded transmission.

RESULTS

Bipolar cell light responses as a function of stimulus frequency

We used temporally flickering light to screen Off bipolar cells for a type that responds at high frequencies. In cb2 cells, a full-field 1 Hz square wave stimulus produced a voltage response that had three components (Figure 1A). The first component, *a*, was the membrane potential, V_m , in the dark (-60.1 ± 5.8 mV, $n = 3$; mean \pm SEM) which was designated as the baseline; the second component, *b*, was the hyperpolarized V_m in the light; and, the third component, *c*, was the transient depolarization at light-off. The peak amplitude of the transient response was 12 – 15 mV relative to the dark baseline level for square wave stimuli over the range of 1 – 16 Hz (Figure 1C; 8 – 14 mV for the average responses in Figure 1D). The 20–80% rise time for the light-off transient, from hyperpolarized level to peak depolarization (30.1 ± 0.7 mV), was 7.2 ± 1.3 ms, with a width at baseline of 21.6 ± 1.5 ms ($n = 5$ responses during the 1 Hz stimulus). Voltage fluctuations were evident but small during a 32 Hz stimulus and were absent during a 333 Hz stimulus, presumably due to flicker fusion in cone phototransduction.

Other Off bipolar cell types lacked a transient light-off response during high frequency flicker. Cb3a/b Off bipolar cells also had a three-component response to a square wave stimulus (Figure 1B; V_m in the dark = -45.3 ± 3.5 mV which is not statistically different from that in cb2 cells; $n = 4$, $p = 0.08$). However, compared to cb2 cells, the responses at light-off rose more slowly (11.8 ± 1.9 ms; $p = 0.002$) and off-transients were reduced to <10% of their peak amplitude during flicker >4 Hz (Figure 1C,D). Thus, cb2 cells have a transient response at light-off during high frequency stimulation that is not present in cb3 cells.

Recovery at the cone to cb2 cell synapse

Off bipolar cells receive excitatory inputs from cone photoreceptors at dendrites in the outer plexiform layer (OPL) and inhibitory inputs from amacrine cells at axon terminals in the inner plexiform layer (IPL). Both inputs can shape the voltage response. To isolate the input from the cone synapse, cb2 bipolar cells were voltage-clamped at -70 mV, the calculated Cl^- reversal potential, and inputs from amacrine cells were blocked by including picrotoxin and strychnine in the bath. Under these conditions, a step of light stopped a continuous inward cb2 cell current (Figure 2A and *inset*). Light-off was followed by an inward transient whose amplitude increased with increasing light step duration. For the bipolar cell in Figure 2A, the peak amplitude of the transient increased to a maximum with a time constant, τ , equal to 90 ms. In a group of 8 cb2 cells, the light-off transient displayed a rapid recovery component with $\tau = 72 \pm 10$ ms (Figure 2B). A rapid transient recovery at light-off is unique to cb2 cells insofar as the transient recoveries in cb3 ($\tau = 744 \pm 22$ ms, $n = 9$) and cb1 ($\tau = 608 \pm 126$ ms, $n = 4$) cells were uniformly slower. We conclude that a rapidly recovering transient is already present in the cb2 cell input at the cone synapse. Moreover, since ground squirrel cones have a monophasic hyperpolarizing response to light (Figure 2, inset; Cao et al., 2014; Kraft, 1988), the synaptic transient originates in the release mechanism and not in a transient cone depolarization.

Instead of using a light step, which changes membrane voltage via a transduction cascade, the transient recovery time course can be directly measured by voltage-clamping a presynaptic cone and a postsynaptic cb2 cell and then using a “two-pulse” paradigm. In this paradigm, a brief cone depolarization from -70 mV depletes a release-competent vesicle pool, while a second identical cone depolarization, given after a variable interval, determines the extent to which the pool is replenished. There is a functional similarity between the interpulse interval of the two pulse paradigm and the duration of a light step (Figure 2, inset). We recorded cb2 cell EPSCs while applying two brief (1 ms) depolarizing pulses to a presynaptic cone. The strength of the cone depolarization was adjusted to produce a maximal cb2 cell response. In one experiment, the first pulse produced a peak response of ~ -440 pA (Figure 2C). After 50 ms, a second pulse produced a response of less than -30 pA, consistent with a marked depletion of the release-competent pool. For comparison, cb2 cell AMPA receptors recover from desensitization with a $\tau \approx 20$ ms (DeVries et al., 2006). As interpulse interval was increased, the amplitude of the second pulse recovered with a $\tau = 69$ ms (Figure 2D). In 35 cone to cb2 cell pairs, the mean recovery τ equaled 125.7 ± 9.6 ms (Figure 2E). Because terminal Ca^{2+} concentrations can affect the ribbon turnover rate (Babai et al., 2010), this sample of 35 cones was subdivided into cones that were depolarized for different lengths of time with different intracellular Ca^{2+} buffers, all of which had statistically similar recovery τ (Table S1). The results show that in cb2 cells, a component of the transient response at light-off (Figure 2A,B) and the 2nd EPSC response (Figure 2C–E) recover with similarly rapid time courses.

In additional experiments, we tested for effects of receptor type and desensitization on the paired-pulse recovery. The synaptic responses of cb3 cells, which make basal contacts with cones, are mediated by both kainate and AMPA receptors (Lindstrom et al., 2014). We used UBP310 (2 μM) to isolate the AMPA receptor-mediated component of the response. The cb3 cell paired-pulse recovery τ , 698 ± 132 ms ($n = 6$ pairs), was significantly slower than that measured at the cone to cb2 cell synapse ($p < 0.0001$, unpaired t test), suggesting that the slow recovery of the light-off response in cb3 cells is not due solely to kainate receptor expression. Recovery was also measured in control and cyclothiazide (CTZ) containing solutions. CTZ increases AMPA receptor affinity and relieves desensitization (Patneau et al., 1993). Paired-pulse τ 's and maximal EPSC amplitudes were unchanged in CTZ (Table S2) while the maximal EPSC response width at half-height was significantly increased (4.2 ± 0.9 fold; paired t test, $p = 0.014$). The results show that the rapid recovery τ at the cone to cb2 cell synapse is not an outcome of receptor desensitization. In addition, the combination of maintained EPSC amplitude and extended duration may signify that receptor saturation occurs in CTZ.

Frequency dependence of synaptic depression

To determine whether rapid replenishment is maintained during multiple cycles of release that are predicted to deplete the entire ribbon-associated pool (Babai et al., 2010; Bartoletti et al., 2010), a cone was stimulated in the loose seal configuration with a train of 1 ms pulses at varying frequencies (Figure 2F,G). An initial 1 ms cone depolarization produced a maximal EPSC in a postsynaptic cb2 cell. We assume that each depolarization depletes the pool of release-competent vesicles and that replenishment takes place during the interval

between depolarizations. At rates of 1 - 4 Hz, all EPSC amplitudes were similar. At rates of 8 - 64 Hz, the peak response amplitude declined after the initial pulse but quickly reached a steady level. A plot of normalized EPSC amplitude (average of the last 8 responses) relative to the first EPSC response was fitted with an exponential curve that had a $\tau = 110$ ms, similar to the τ obtained from a two pulse experiment in the same pair ($\tau = 75$ ms; Figure 2H). Comparable results were obtained from 6 cone to cb2 cell pairs (paired pulse $\tau = 91.1 \pm 12.8$ ms versus pulse frequency $\tau = 137.6 \pm 45.1$ ms; values are not statistically different by a paired *t* test; $p = 0.058$). We conclude that recovery at the cone to cb2 cell synapse occurs with a τ of about 130 ms which is equivalent to a 37% reduction in transient peak amplitude at a frequency of ~ 7.5 Hz. This reduction in peak amplitude, which occurs during both pulse pairs and longer trains, is similar to the decrease in the cb2 transient amplitude during square wave light at 8 Hz (Figure 1A,C,D).

The time course of presynaptic recovery

The 130 ms recovery τ , if attributed to presynaptic vesicle replenishment, implies a steady vesicle fusion rate of $\sim 3100 \text{ s}^{-1}$ ($1/0.13 \text{ s} \times 400$ docking sites per cone). This value greatly exceeds the measured release rates in salamander ($\sim 500 \text{ vesicles-s}^{-1}$; (Sheng et al., 2007)), lizard (~ 400 (Choi et al., 2005)), and ground squirrel (~ 1000 (DeVries et al., 2006)) cones. To determine whether postsynaptic recovery τ accurately represents the presynaptic replenishment τ , we modified the paired pulse experiment so that we could simultaneously measure the EPSC and the H^+ block of the Ca^{2+} current (DeVries, 2001). At bipolar cell ribbons, the H^+ block of the Ca^{2+} current is proportional to the amount of vesicle fusion as shown by capacitance measurements (Palmer et al., 2003). The cb2 EPSC was measured during two 15 ms steps from -70 to -30 mV (Figure 3A, upper traces) and recovered with $\tau = 50$ ms (Figure 3B, red circles). The H^+ block of the cone Ca^{2+} current was measured during the same series of pulses as the first step response minus the second (Figure 3, *inset* (DeVries, 2001)). At short interpulse intervals, when only a small fraction of the presynaptic vesicle pool is recharged, the H^+ block was small or absent during the second pulse and the cone difference current was maximal (Figure 3A, lower traces). With increasing interpulse interval, the H^+ block recovered so that the shape of the current during the second pulse approached that of the first pulse and the difference current became smaller. In the plot shown in Figure 3B, the H^+ block recovered with a $\tau = 410$ ms. In a total of 6 pairs (Figure 3C), the recovery τ for the cb2 EPSC response (98 ± 21 ms) was faster than that of the H^+ block (332 ± 57 ms; significantly different at $p = 0.0094$; paired *t* test). In a larger sample of cones that were not paired with a cb2 cell, the recovery from proton block occurred with a $\tau = 448.7 \pm 28.2$ ms ($n = 58$). Subsets of cones were recorded in HEPES buffer (5 mM) to reduce the likelihood of proton block saturation ($\tau = 474.9 \pm 43.8$ ms, $n = 16$), in TBOA (100 - 200 μM) to block the activation of a transporter anion conductance by released glutamate ($\tau = 470.6 \pm 35.7$ ms, $n = 43$), and during β -escin perforated patch recordings that minimized rundown ($\tau = 556.2 \pm 83$ ms, $n = 11$; differences were not significant at the $p < 0.05$ level; Wilcoxon rank sum test; recovery in some cones was measured under several conditions). The results suggest that the cb2 cell EPSC recovers faster than the cone release-competent vesicle pool, a mismatch that can occur if receptor saturation limits the size of the postsynaptic response so that a partial presynaptic recovery is associated with a full postsynaptic recovery (Figure 3D).

EPSC amplitude and cone membrane capacitance change

To better compare the time courses of presynaptic vesicle replenishment and postsynaptic EPSC recovery, we simultaneously measured cone membrane capacitance (C_m) and cb2 cell EPSC response. We first confirmed in a two pulse experiment that replenishment at the cone terminal is relatively slow. Two examples (Figures 4A,B) show depolarization-evoked C_m jumps of 15.0 and 13.2 fF preceding intervals of 200 and 500 ms, respectively. After the intervals, a second step led to smaller jumps of 6.5 and 6.6 fF, respectively. Changes in membrane (G_m) and pipette (G_s) conductance, that can obscure changes in C_m , were not observed. Average responses (Figure 4C; $n = 6$ cones) were used to plot C_m versus interpulse interval (Figure 4D), which was fitted with a saturating exponential to give a τ of 0.7 – 1.1 s. Thus, the cone C_m recovery τ was slower than the recovery τ for EPSCs and comparable to that obtained by measuring the H^+ block.

If receptor saturation limits EPSC amplitude, then a range of depolarizing stimuli should increase cone transmitter release without concomitantly increasing cb2 cell EPSC amplitude. To identify this range, we compared presynaptic capacitance jumps to postsynaptic EPSC responses during paired recordings (Figure 5). To generate a variety of response amplitudes, we depolarized the cone with a pair of 1 ms pulses separated by an interval of 500 ms, which is slightly less than the τ for cone recovery. The first pulse was either to -40 , -30 , -10 or $+30$ mV, and sometimes released only a portion of the presynaptic pool, and the second pulse was always to -10 mV. EPSCs differed in amplitude but not shape (Figure 5B), so we used amplitude as a measure of response strength. C_m and corresponding peak EPSC amplitudes were individually compared. Figure 5A shows the results from a single pair. In this experiment, the largest individual C_m and EPSC responses, ~ 20 fF and ~ -400 pA, were obtained during steps to -10 mV that were either first in the sequence or second and not preceded by an EPSC response. On average, first steps to -10 and $+30$ mV produced the largest capacitance jumps, with C_m values of 15.0 ± 1.4 and 13.3 ± 1.9 fF ($n = 9$ pairs), respectively. Corresponding EPSCs were -382 ± 21 and -366 ± 20 pA. A step to -30 mV elicited a much smaller capacitance jump (2.3 fF) and a still substantial EPSC of -253 pA. Overall, steps to -30 mV elicited a fivefold smaller than maximum C_m , 2.2 ± 0.3 fF, and a peak EPSC response of -179 ± 31 pA, which was only twofold smaller than that obtained during the steps to $+30$ and -10 mV.

A plot of EPSC amplitude versus C_m (Figure 5C) obtained from the pair shown in Figure 5A showed a steep increase in peak current as a function of C_m in the range of 0 – 5 fF. For larger capacitance jumps, EPSC amplitude leveled off. The plot in Figure 5D summarizes results from 9 cone to cb2 cell pairs. By ~ 2 fF, the EPSC had reached half-maximal saturation, and by ~ 5 fF the response was 80% of its maximum. An average maximal capacitance jump of 15 fF corresponds to roughly 15 vesicles fusing per ribbon (assuming 0.05 fF per vesicle (Neef et al., 2007) and ~ 20 ribbons per terminal (Li and DeVries, 2006)), while 50% and 80% EPSC responses correspond to 2 and 5 fused vesicles per ribbon, respectively. The results show that AMPA receptors at the cone to cb2 cell synapse saturate during a strong cone stimulus.

A weak antagonist relieves receptor saturation at the cone to cb2 cell synapse

Weak competitive antagonists allow receptors to respond to increases in glutamate concentration at levels that would normally be saturating (Chanda and Xu-Friedman, 2010; Diamond and Jahr, 1997; Neher and Sakaba, 2001; Wadiche and Jahr, 2001). Paired pulse recovery was measured both in control and in a weak antagonist containing solution (kynurenic acid; KYN, 1–4 mM). KYN (2 mM; Figure 6A,B) reduced the maximal EPSC amplitude by 50% and prolonged the cb2 cell EPSC recovery time course ($\tau = 426$ versus 155 ms; Figure 6C). Pairwise comparisons (Figure 6D) showed a statistically significant 3.9 \pm 1.3-fold increase in recovery τ (KYN versus control, $n = 4$ pairs, $p = 0.022$; paired t test; $\tau = 135 \pm 25$ ms in control and 440 ± 60 ms in KYN). Critically, the EPSC amplitudes in KYN continued to increase at interpulse intervals where the recovery in control had neared its maximum value (Figure 6A–C). Between 0.4 and 1.0 s, the second EPSCs in KYN increased by $46.9 \pm 12.0\%$ while the corresponding EPSCs in control increased by only $7.3 \pm 2.0\%$ (significantly different by unpaired t test; $p = 0.017$). An increase in the EPSC amplitude in the presence of weak antagonist without a comparable increase in control is consistent with relief of receptor saturation.

We next used KYN to examine whether receptors saturate during a light response. For these experiments, we compared the effect of 1 mM KYN on the amplitudes of the light-off transients after 0.2 and 1.0 s steps. We chose pulse intervals that were associated with similar amplitude EPSCs in control (Figure 2A), but which might produce different peak glutamate concentrations based on the τ for refilling of the cone vesicle release pool. In one cb2 cell, the average control light-off EPSC amplitude increased by 2% between the 0.2 and 1.0 s pulses, whereas the the EPSCs in KYN increased by 2.8-fold (Figure 6E, upper). A small increase in the amplitude of the control EPSC accompanied by a large change in the amplitude of the EPSC in KYN is consistent with receptor saturation during the second light-off response. Similar results were obtained in a total of 6 cells where the amplitude ratios of the first and second EPSCs in control were not significantly different ($\text{EPSC}_{0.2} = -168.5 \pm 15.6$ pA, $\text{EPSC}_{1.0} = -216.6 \pm 31.7$ pA, $p = 0.10$; paired t test). In the same cells, KYN reduced the size of the light-off transient following a 0.2 s step by $63.5 \pm 5.7\%$ (-60.3 ± 9.5 versus -168.4 ± 15.6 pA; $p = 0.0001$), but did not affect the EPSC amplitude following a 1s light step (-220.9 ± 35.7 versus -216.6 ± 31.7 pA; $p = 0.86$). The peak current blocked by KYN was also significantly different between the 0.2 and 1.0 s pulses ($p = 0.0009$; Figure 6F). As a control, we presented the same light steps in the presence of CNQX (0.4 μM), a strong AMPA receptor antagonist that should reduce the amplitude of the transient by the same amount irrespective of light duration. In an individual recording, CNQX suppressed the light-off transient by 53 and 61% after the 0.2 and 1.0 s steps, respectively (Figure 6E). In 9 recordings, transient amplitudes in CNQX were reduced by $41.2 \pm 5.5\%$ and $34.4 \pm 7.9\%$ following 0.2 and 1.0 s steps, respectively (p values for 0.2 and 1.0 s flashes different from control = 0.0005 and 0.007, different from each other = 0.177). The results are consistent with the idea that the glutamate concentrations at cb2 cell receptors approach saturation during the transient that follows a 1.0 s light pulse.

Monte Carlo simulation of transmission

We used a Monte Carlo simulation (Stiles and Bartol, 2001) to investigate the relationship between the number of transmitter quanta released at a ribbon and the saturation of cb2 cell AMPA receptors. The first task was to specify synapse geometry (Figure 7A,B and S1). Importantly, we chose a ribbon-base length of 750 nm from a range of 200 – 1000 nm (Sterling and Matthews, 2005). An EM reconstruction of a cone ribbon with a similar length docked 36 vesicles (Sterling and Matthews, 2005). The kinetic model describing the cb2 receptor response to glutamate was modified from Häusser and Roth (1997). Specifically, the rate constants involving glutamate binding were increased to account for a small difference in EC_{50} between cb2 and Purkinje cell AMPARs (340 versus 440 μM , respectively (DeVries et al., 2006; Häusser and Roth, 1997; Figure S2). We tested the simulation by releasing a single vesicle at a distance of 180 nm (DeVries et al., 2006) from the model cb2 receptor array and then comparing the time course of simulated and actual small EPSCs. The simulated glutamate concentration at the receptor array peaked at 500 μM , 25 μs after release. The actual and simulated EPSC time courses were similar with the largest deviations occurring during the response decay (Figure S3). We next simulated the simultaneous release of 1–36 docked vesicles. A plot of normalized EPSC amplitude versus the number of released vesicles (Figure 7C) showed saturation for invaginating but not basal contacts. The cb2 cell EPSC response was ~50% saturated when 2.5 vesicles were released, matching the capacitance results. We varied the number of glutamate molecules per vesicle (2000 – 5000) and the transmitter diffusion constant ($0.1 - 1.0 \text{ cm}^2\text{-s}^{-1}$) and found that saturation was robust to these uncertainties (Figure S4).

To more closely approximate conditions during a light response, we released vesicles with temporal jitter. We selected vesicle release times according to a probability distribution derived from the rising phase of the cone Ca^{2+} current (Figure S5). The resulting simulated EPSCs had a time course similar to our light response data (Figure 7D). With the increased release spread, the maximal response occurred at higher vesicle numbers, but a 50% maximal response was still achieved with fewer than 5 released vesicles (Figure 7E), and receptors approached 80 – 90% of their saturated response when 20 – 25 vesicles/ribbon were released. The simulations support the idea that cb2 receptors display a saturating non-linearity under both experimental and physiological conditions.

DISCUSSION

The perception of a rapidly changing visual stimulus is limited by the frequencies signaled at the cone synapse. Primate horizontal and ganglion cells can process 80-100 Hz flicker (Derrington and Lennie, 1984; Smith et al., 2001), but moderate (~0.2 Hz) rates of vesicle refilling of the release pool at the cone ribbon motivated us to address the question: how do cone ribbons signal high temporal frequencies to postsynaptic bipolar cells?

Behavioral and functional tests in the ground squirrel suggest that the sensitivity to high frequency flicker equals or exceeds that in humans (Jacobs et al., 1980; Tansley, 1965). Correspondingly, ground squirrel cone light responses are 30–50% faster than those of primate cones (Cao et al., 2014; Kraft, 1988). The bipolar cells that mediate high frequency signaling in the ground squirrel retina have not been identified, but the cb2 cell is a

candidate. The cb2 cell stands out because it has a transient depolarization at light-off that exceeds the baseline voltage at 16 Hz and is still prominent at 32 Hz (Figure 1). Additionally, cb2 cells have dendrites that are close to the sites of ribbon-mediated transmitter release within invaginations (DeVries et al., 2006); express AMPA receptors that recover rapidly from desensitization ($\tau = \sim 20$ ms; DeVries, 2000); and, contain the GluA4 subunit (Lindstrom et al., 2014), which is associated with rapid transmission (Koike-Tani et al., 2005). On investigating the interval dependence of the transient response at the cone to cb2 cell synapse, we found a paradoxical difference between the time courses of presynaptic refilling and postsynaptic recovery. The postsynaptic recovery τ was 130 ms (Figure 2), whereas the presynaptic replenishment τ was 500 – 1000 ms (Figures 3, 4). Simultaneous cb2 cell EPSC and cone capacitance measurements resolved this paradox by showing that the coordinated fusion of cone vesicles could produce postsynaptic receptor saturation (Figure 5), consistent with a Monte Carlo model (Figure 7). Experiments with a weak antagonist further suggested that saturation can occur following a light stimulus (Figure 6) and acts to speed up the apparent recovery time course of the off transient (Figure 2). Hence, by limiting the dynamic range of signaling, the cone to cb2 cell synapse counteracts ribbon depression.

Alternative mechanisms for the rapid recovery of the cb2 cell transient

The Off cone bipolar cell types have different temporal light responses (Baden et al., 2013; Ichinose and Hellmer, 2015). These differences can originate from the cone synapse (DeVries, 2000), from voltage-dependent currents in the bipolar cell membrane (Ichinose et al., 2005; Ma et al., 2005; Puthussery et al., 2013; Saszik and DeVries, 2012), from inhibitory inputs at the bipolar cell terminal (Eggers and Lukasiewicz, 2011), or from a combination. The rapid recovery that we demonstrate originates in a specialized mechanism at the cone synapse because it persists when the bipolar cell is voltage-clamped and bathed in drugs that block amacrine cell synapses. In current clamp without blockers, the transient at light-off may be enhanced or shaped by a momentary gap in inhibition at amacrine to bipolar cell synapses in the inner retina (Dong and Werblin, 1998; Lagnado, 1998). In addition, transient Off bipolar cell types in the mouse (Ma et al., 2005; Baden et al., 2013) and primate (Puthussery et al., 2013), but not the ground squirrel (Saszik and DeVries, 2012), express a voltage-dependent Na^+ current or another transient generating mechanism (Baden et al., 2013) that may amplify the responses at the cone synapse. Taken together, these results suggest that a combination of mechanisms may support high frequency signaling in Off bipolar cells.

Relationship between synapse saturation, gain, and frequency response

For small cone depolarizations, the cb2 cell synapse has a relatively steep relationship between the number of released vesicles and the EPSC response (Figure 5). We extended our model to further examine the signaling function of this high-gain region of the input-output curve. A simple model assumes a square wave light stimulus with a high cone release rate in the dark, zero release in bright light, and a τ that characterizes the refilling of the docked pool of vesicles during the half period in bright light. The model further assumes that there are 20 vesicle docking sites per ribbon, and that n repopulated vesicle sites undergo synchronous release at light-off. For the model to be useful, we need to posit a bipolar cell

threshold for transmitter release onto ganglion cells followed by an estimate of how many cone vesicles must be released at light-off in order to depolarize the bipolar cell to threshold. We assign a bipolar cell threshold of 2 – 3 mV relative to the resting level in bright light, and estimate from the light response amplitude (30.7 mV; Figure 1A) and the input-output curve ($C_{m(1/2)}$ equivalent to 2.3 vesicles per ribbon; Figure 5D) that bipolar cell threshold is reached when n equals 0.3 – 0.45 vesicles per ribbon (see supplemental experimental procedures).

The highest temporal frequency signaled in bright light, f_{Max} , corresponds to the time that recharges just enough vesicles per ribbon, n , to produce a threshold response in the bipolar cell. We can relate $n/20$ to f_{Max} by

$$f_{Max} = \left(-2 \tau \ln \left(1 - \frac{n}{20} \Big|_{Threshold} \right) \right)^{-1}$$

The maximum signaling frequency increases by reducing the response threshold, n , equivalent to an increase in gain, or by decreasing the vesicle refilling τ . Using a replenishment $\tau = 0.7$ s and an $n = 0.30 - 0.45$, we arrive at an $f_{Max} = 31 - 47$ Hz. This frequency range is likely an underestimate because it relies on average values that might include cells whose synaptic responses have started to rundown during whole cell recording. If instead we use the $C_{m(1/2)}$ value from the experiment shown in Figure 5A–C, which is equivalent to 1.44 vesicles per ribbon (equal to 0.19 – 0.28 vesicles per ribbon at threshold) and a replenishment τ of 0.5, representative of the τ obtained from proton block measurements, then $f_{Max} = 70 - 105$ Hz. The relationship between f_{Max} , response threshold, and replenishment τ is plotted in Figure 7E over the range of interest for the cone synapse. Several observations support the higher frequency range: the amplitude of the 32 Hz square wave response (Figure 1A) was 7.6 ± 0.5 mV, substantially greater than the benchmark 2 – 3 mV threshold; the synapse itself can signal frequencies exceeding 64 Hz (Figure 2F,G); and a light-off transient recovery $\tau = 90$ ms (Figure 2A) is equivalent to a frequency of 54 – 82 Hz, assuming a threshold of 2 – 3 mV and a 30.7 mV peak response. Alternatively, if the frequency range of the individual bipolar cell is indeed lower than the behavioral or ganglion cell limit, summation in the inner retina at the bipolar to ganglion cell synapse may extend the perceptual range to higher frequencies. While containing some uncertainties, our simple model shows how a high gain synaptic response can encode a high frequency light stimulus. Examined from the point of view of high frequency transmission, synapse saturation at low frequencies is an outcome of building a high gain synapse.

Receptor saturation during a physiological stimulus

cb2 cell receptors saturate when vesicles are synchronously released during a cone step in voltage clamp (Figure 5). However, cone depolarization after a light pulse has a relatively slow rise time (~5 ms) that should produce a staggering of vesicle release and a reduction of the peak glutamate concentration. We used a weak antagonist, KYN, to investigate saturation during a light response. In paired recordings, KYN increased the recovery τ from an average of 135 to 440 ms. A prolonged recovery time course, especially at long interpulse

intervals when the control EPSC has reached a steady level, is consistent with relief from receptor saturation. EPSC responses following light steps of 0.2 and 1.0 s had similar amplitudes in control, but were also differently blocked by 1 mM KYN (Figure 6E,F), consistent with a prolongation of the recovery τ and saturation following the 1.0 s step. Weak antagonists such as KYN effectively reduce the affinity of the receptor for glutamate allowing the receptor to respond to concentrations that would normally be saturating. This effect of KYN is concentration dependent: The recovery τ should be nearly unchanged (i.e., 135 ms) in very low concentrations of KYN insofar as saturation still occurs. In relatively high concentrations of KYN, the recovery τ should approach the presynaptic refilling τ (0.7 – 1.1 s). The measured τ in 1 – 4 mM KYN, 440 ms, is in the middle of this range. By relieving saturation and prolonging the recovery time course, KYN lengthens the time required for the postsynaptic response in the bipolar cell to reach threshold for release onto postsynaptic ganglion cells, thereby reducing the frequency bandwidth of the pathway.

Our results supporting AMPA receptor saturation during light differ from those at the rod bipolar to AII amacrine cell synapse (Dunn and Rieke, 2008), but are similar to those at the bipolar to ganglion cell synapse (Chen and Diamond, 2002; Sagdullaev et al., 2006). A different type of saturation occurs at the rod to rod bipolar cell synapse during steady glutamate release in the dark. At this synapse, saturation occurs within a G protein cascade that links metabotropic glutamate receptors to membrane ion channels, introducing a threshold non-linearity (Sampath and Rieke, 2004).

Versatile processing at retinal ribbons

A recent idea is that retinal ribbon synapses are versatile processing units that can perform different functions depending on the wiring of their local circuit. The key to this versatility is the causal link between tonic replenishment and phasic release. Depression at bipolar cell ribbons plays a role in luminance and contrast adaptation (Kastner and Baccus, 2014; Oesch and Diamond, 2011) and in encoding the full 10 – 12 log units of intensity over which natural stimuli vary (Euler and Masland, 2000; Kastner and Baccus, 2014; Singer and Diamond, 2006). In these roles, the fraction of docking sites that contain release-competent vesicles is adjusted to maintain coding efficiency while avoiding saturation in the signaling pathway. Even when AMPA receptor saturation occurs at the On bipolar to ganglion cell synapse, NMDA receptors are recruited to maintain the dynamic range (Chen and Diamond, 2002; Sagdullaev et al., 2006). Our results also rely on the causal link between tonic replenishment and phasic release but illustrate an opposing idea which is that saturation at cb2 cell contacts can improve temporal performance at the expense of dynamic range and coding efficiency.

Versatility is also characteristic of the cone synapse, where a single output provides input to as many as 14 bipolar cell types, a number of which have distinctive temporal responses. Indeed, a recent study in the mouse (Kim et al., 2014) shows how a subtle interplay between transient and sustained bipolar cell responses can produce directional responses in starburst amacrine cell neurites. In their model, a sustained bipolar cell such as the mouse type 1 or 4 or the ground squirrel cb3 makes axonal contacts with the central regions of a starburst cell's neurites while transient responding bipolar cells such as the mouse type 3a or 3b and the

ground squirrel cb2 contact starburst cell processes more peripherally. The result is that a centrifugally moving bar of light creates a temporal sequence of excitatory inputs that reinforce each other along the neurite, eliciting transmitter release from the neurite tips onto the dendrites of directionally selective ganglion cells. This model illustrates how the high frequency transients at the cone to cb2 cell synapse may interact with more sustained bipolar cell responses to bring about complex temporal processing in the inner retina.

In the mammalian retina, the majority medium/long-wavelength sensitive cones provide input to almost all of the bipolar cell types. A high vesicle replenishment rate at the cone photoreceptor synapse in the dark would insure that all types can signal at the highest temporal frequencies, but with a metabolic cost. However, most ganglion cell types do not carry high frequency information (Baden et al., 2016), and thus the metabolic cost can be lowered by reducing the ribbon replenishment rate while at the same time creating specialized synaptic contacts that can convey and amplify high frequency components at the expense of dynamic signaling range.

MATERIALS & METHODS

Preparation and Electrophysiology

Procedures were approved by the Northwestern University Animal Care and Use Committee. The procedure for making ground squirrel (*Ictidomys tridecemlineatus*) retinal slices has been described (DeVries et al., 2006; DeVries and Schwartz, 1999). For experiments involving light responses, retinal slices were obtained under dim red illumination (Saszik and DeVries, 2012) and visualized under infra-red illumination with a Zeiss Axioskop-2FS microscope using a 63x water immersion objective. Recordings were made with Axopatch 200B amplifiers (Molecular Devices). Signals were filtered at 5 kHz and digitized at 10 kHz with a HEKA ITC-18 (HEKA Elektronik) operated with custom software (Igor Pro 6.1; WaveMetrics). Patch pipettes were pulled from borosilicate glass capillary tubes to tip resistances of 8–12 M Ω .

The external solution consisted of (in mM): NaCl 115, KCl 3.1, MgSO₄ 2.5, glucose 6, Na-succinate 1, Na-malate 1, Na-lactate 1, Na-pyruvate 1, CaCl₂ 2, and NaHCO₃ 25, 0.05% phenol red, and was equilibrated with 5% CO₂/95% O₂ to a pH of 7.4. Picrotoxin (50 μ M) and strychnine (10 μ M) were included in the bath during voltage but not current clamp recordings. The patch pipette solution for both the cone and bipolar cell during cell pair recordings contained (in mM): KCl 120, Cs-EGTA 10, MgSO₄ 5, HEPES 10, ATP 5 and GTP 0.5; pH 7.3 with KOH. For experiments that measured bipolar cell light responses, the first two components of the solution were changed: K-methylsulfate 112, KCl 8, and K-EGTA 10. For cone capacitance measurements, the first component was changed: CsCl 112, KCl 8, and pH was adjusted with CsOH. Intracellular solutions contained either Alexa Fluor 488 (0.2 mM; Invitrogen) or 0.5% Neurobiotin (Vector Laboratories) for subsequent visualization of cones and bipolar cells in fixed slices using immunohistochemistry. Solutions were corrected to 285 \pm 5 mOsm. Experiments were performed at 32 – 33 $^{\circ}$ C which is 4 – 5 $^{\circ}$ C lower than non-hibernating body temperature. Although glutamate transporters have a Q₁₀ of ~3, this temperature difference should not affect cone cleft glutamate concentrations during a brief EPSC insofar as the putative cone transporter,

EAAT5, has a relatively slow turnover rate (~1 s; Gameiro et al, 2011) and the processes of EAAT1-expressing Müller glial cells surround cones but do not enter the cleft. Chemicals were obtained from Sigma-Aldrich unless indicated. Values are mean \pm SEM. Retinas were stimulated with a 574 nm LED attached to a microscope video port. LED intensity was controlled by pulse-width modulation and calibrated with a photodiode detector (International Light) positioned beneath the microscope objective. Intensity was converted to photons at the λ_{\max} (520 nm) for the ground squirrel green cone pigment (Kraft, 1988).

Membrane capacitance measurements

Membrane capacitance was measured with a HEKA EPC-10 using the 'sine+dc' Lockin routine in Patchmaster software. A 1 kHz sinusoidal voltage command (mean = -70 ± 10 mV) was applied during two 0.5 s periods that were separated by an interval consisting, in sequence, of a 20 ms pause, a 1 ms depolarization, and a 20 ms pause. Traces were sampled at 20 kHz and low-pass filtered at 2.8 kHz. Whole cell pipette tips were coated with Sylgard and access resistance was 20 – 25 M Ω . TBOA (400 μ M; Tocris Bioscience) and CsCl (5 mM) were added to the external solution to block the cone glutamate transporter and I_h , respectively. For paired recordings, bipolar cell membrane potential was maintained at -70 mV with an Axopatch 200B.

Synapse model

The model synapse was constructed using Blender 2.49 (www.blender.org) and imported into MCell 3 for the Monte Carlo simulation (Kerr et al., 2008; Stiles and Bartol, 2001). The model structure (Figures 7A,B and S1) was based on published EM reconstructions of the cone terminal. For details about both the dimensions of the synapse model and the number and location of glutamate receptors, see supplemental experimental procedures. For the Monte Carlo simulation, time steps were 1 μ s and data points were averages from 50 independent runs. Vesicles contained 4000 glutamate molecules unless stated (see supplemental experimental procedures for justification). The glutamate diffusion constant was 0.33×10^{-5} cm²-s⁻¹ (Nielsen et al., 2004) unless stated. The AMPA receptor model was adapted from Häusser and Roth (1997). To address receptor saturation, which depends largely upon glutamate affinity and less upon the decay phase of the EPSC, we first modified the rate constants to decrease the EC₅₀ for glutamate from 440 to 340 μ M (Figure S2A). Without further adjustment, both the rise and decay of the simulated mEPSC were slower than the rise and decay of the cb2 cell mEPSC. To match the rising phase, the scheme was further modified (Figure S2B).

Supplementary Material

Refer to Web version on PubMed Central for supplementary material.

ACKNOWLEDGEMENTS

Supported by EY012141 (S.H.D.) and Research to Prevent Blindness.

References

- Babai N, Bartoletti TM, Thoreson WB. Calcium regulates vesicle replenishment at the cone ribbon synapse. *J Neurosci*. 2010; 30:15866–15877. [PubMed: 21106825]
- Baden T, Berens P, Bethge M, Euler T. Spikes in mammalian bipolar cells support temporal layering of the inner retina. *Curr Biol*. 2013; 23:48–52. [PubMed: 23246403]
- Baden T, Berens P, Franke K, Roman Roson M, Bethge M, Euler T. The functional diversity of retinal ganglion cells in the mouse. *Nature*. 2016; 529:345–350. [PubMed: 26735013]
- Bartoletti TM, Babai N, Thoreson WB. Vesicle pool size at the salamander cone ribbon synapse. *J Neurophysiol*. 2010; 103:419–423. [PubMed: 19923246]
- Cao LH, Luo DG, Yau KW. Light responses of primate and other mammalian cones. *Proc Natl Acad Sci U S A*. 2014; 111:2752–2757. [PubMed: 24550304]
- Chanda S, Xu-Friedman MA. A low-affinity antagonist reveals saturation and desensitization in mature synapses in the auditory brain stem. *J Neurophysiol*. 2010; 103:1915–1926. [PubMed: 20107122]
- Chen S, Diamond JS. Synaptically released glutamate activates extrasynaptic NMDA receptors on cells in the ganglion cell layer of rat retina. *J Neurosci*. 2002; 22:2165–2173. [PubMed: 11896156]
- Choi SY, Borghuis BG, Rea R, Levitan ES, Sterling P, Kramer RH. Encoding light intensity by the cone photoreceptor synapse. *Neuron*. 2005; 48:555–562. [PubMed: 16301173]
- Chun MH, Grunert U, Martin PR, Wassle H. The synaptic complex of cones in the fovea and in the periphery of the macaque monkey retina. *Vision Res*. 1996; 36:3383–3395. [PubMed: 8977005]
- Cleland BG, Dubin MW, Levick WR. Sustained and transient neurones in the cat's retina and lateral geniculate nucleus. *J Physiol*. 1971; 217:473–496. [PubMed: 5097609]
- Derrington AM, Lennie P. Spatial and temporal contrast sensitivities of neurones in lateral geniculate nucleus of macaque. *J Physiol*. 1984; 357:219–240. [PubMed: 6512690]
- DeVries SH. Bipolar cells use kainate and AMPA receptors to filter visual information into separate channels. *Neuron*. 2000; 28:847–856. [PubMed: 11163271]
- DeVries SH. Exocytosed protons feedback to suppress the Ca²⁺ current in mammalian cone photoreceptors. *Neuron*. 2001; 32:1107–1117. [PubMed: 11754841]
- DeVries SH, Li W, Saszik S. Parallel processing in two transmitter microenvironments at the cone photoreceptor synapse. *Neuron*. 2006; 50:735–748. [PubMed: 16731512]
- DeVries SH, Schwartz EA. Kainate receptors mediate synaptic transmission between cones and 'Off' bipolar cells in a mammalian retina. *Nature*. 1999; 397:157–160. [PubMed: 9923677]
- Diamond JS, Jahr CE. Transporters buffer synaptically released glutamate on a submillisecond time scale. *J Neurosci*. 1997; 17:4672–4687. [PubMed: 9169528]
- Dong CJ, Werblin FS. Temporal contrast enhancement via GABAC feedback at bipolar terminals in the tiger salamander retina. *J Neurophysiol*. 1998; 79:2171–2180. [PubMed: 9535976]
- Dowling JE, Boycott BB. Organization of the primate retina: electron microscopy. *Proc R Soc Lond B Biol Sci*. 1966; 166:80–111. [PubMed: 4382694]
- Dunn FA, Rieke F. Single-photon absorptions evoke synaptic depression in the retina to extend the operational range of rod vision. *Neuron*. 2008; 57:894–904. [PubMed: 18367090]
- Eggers ED, Lukasiewicz PD. Multiple pathways of inhibition shape bipolar cell responses in the retina. *Vis Neurosci*. 2011; 28:95–108. [PubMed: 20932357]
- Euler T, Masland RH. Light-evoked responses of bipolar cells in a mammalian retina. *J Neurophysiol*. 2000; 83:1817–1829. [PubMed: 10758094]
- Foster KA, Kreitzer AC, Regehr WG. Interaction of postsynaptic receptor saturation with presynaptic mechanisms produces a reliable synapse. *Neuron*. 2002; 36:1115–1126. [PubMed: 12495626]
- Gameiro A, Braams S, Rauen T, Grewer C. The discovery of slowness: low-capacity transport and slow anion channel gating by the glutamate transporter EAAT5. *Biophys J*. 2011; 100:2623–2632. [PubMed: 21641307]
- Grabner CP, Zenisek D. Amperometric resolution of a prespike stammer and evoked phases of fast release from retinal bipolar cells. *J Neurosci*. 2013; 33:8144–8158. [PubMed: 23658155]
- Harrison J, Jahr CE. Receptor occupancy limits synaptic depression at climbing fiber synapses. *J Neurosci*. 2003; 23:377–383. [PubMed: 12533597]

- Hausser M, Roth A. Dendritic and somatic glutamate receptor channels in rat cerebellar Purkinje cells. *J Physiol.* 1997; 501:77–95. [PubMed: 9174996]
- Helmstaedter M, Briggman KL, Turaga SC, Jain V, Seung HS, Denk W. Connectomic reconstruction of the inner plexiform layer in the mouse retina. *Nature.* 2013; 500:168–174. [PubMed: 23925239]
- Hopkins JM, Boycott BB. The cone synapses of cone bipolar cells of primate retina. *J Neurocytol.* 1997; 26:313–325. [PubMed: 9192295]
- Ichinose T, Hellmer CB. Differential Signalling and Glutamate Receptor compositions in the OFF Bipolar Cell Types in the Mouse Retina. *J Physiol.* 2015; 594:883–894. [PubMed: 26553530]
- Ichinose T, Shields CR, Lukasiewicz PD. Sodium channels in transient retinal bipolar cells enhance visual responses in ganglion cells. *J Neurosci.* 2005; 25:1856–1865. [PubMed: 15716422]
- Innocenti B, Heidelberger R. Mechanisms contributing to tonic release at the cone photoreceptor ribbon synapse. *J Neurophysiol.* 2008; 99:25–36. [PubMed: 17989244]
- Jackman SL, Choi SY, Thoreson WB, Rabl K, Bartoletti TM, Kramer RH. Role of the synaptic ribbon in transmitting the cone light response. *Nat Neurosci.* 2009; 12:303–310. [PubMed: 19219039]
- Jacobs GH, Blakeslee B, Mccourt ME, Tootell RBH. Visual Sensitivity of Ground-Squirrels to Spatial and Temporal Luminance Variations. *Journal of Comparative Physiology.* 1980; 136:291–299.
- Kastner DB, Baccus SA. Insights from the retina into the diverse and general computations of adaptation, detection, and prediction. *Curr Opin Neurobiol.* 2014; 25:63–69. [PubMed: 24709602]
- Kerr RA, Bartol TM, Kaminsky B, Dittrich M, Chang JC, Baden SB, Sejnowski TJ, Stiles JR. Fast Monte Carlo Simulation Methods for Biological Reaction-Diffusion Systems in Solution and on Surfaces. *SIAM J Sci Comput.* 2008; 30:3126–3149. [PubMed: 20151023]
- Kim JS, Greene MJ, Zlateski A, Lee K, Richardson M, Turaga SC, Purcaro M, Balkam M, Robinson A, Behabadi BF, et al. Space-time wiring specificity supports direction selectivity in the retina. *Nature.* 2014; 509:331–336. [PubMed: 24805243]
- Koike-Tani M, Saitoh N, Takahashi T. Mechanisms underlying developmental speeding in AMPA-EPSC decay time at the calyx of Held. *J Neurosci.* 2005; 25:199–207. [PubMed: 15634782]
- Kraft TW. Photocurrents of cone photoreceptors of the golden-mantled ground squirrel. *J Physiol.* 1988; 404:199–213. [PubMed: 3253431]
- Lagnado L. Retinal processing: amacrine cells keep it short and sweet. *Curr Biol.* 1998; 8:R598–600. [PubMed: 9742387]
- Li W, DeVries SH. Bipolar cell pathways for color and luminance vision in a dichromatic mammalian retina. *Nat Neurosci.* 2006; 9:669–675. [PubMed: 16617341]
- Light AC, Zhu Y, Shi J, Saszik S, Lindstrom S, Davidson L, Li X, Chiodo VA, Hauswirth WW, Li W, DeVries SH. Organizational motifs for ground squirrel cone bipolar cells. *J Comp Neurol.* 2012; 520:2864–2887. [PubMed: 22778006]
- Lindstrom SH, Ryan DG, Shi J, DeVries SH. Kainate receptor subunit diversity underlying response diversity in retinal off bipolar cells. *J Physiol.* 2014; 592:1457–1477. [PubMed: 24396054]
- Ma YP, Cui J, Pan ZH. Heterogeneous expression of voltage-dependent Na⁺ and K⁺ channels in mammalian retinal bipolar cells. *Vis Neurosci.* 2005; 22:119–133. [PubMed: 15935105]
- Mennerick S, Matthews G. Ultrafast exocytosis elicited by calcium current in synaptic terminals of retinal bipolar neurons. *Neuron.* 1996; 17:1241–1249. [PubMed: 8982170]
- Neef A, Khimich D, Piriš P, Riedel D, Wolf F, Moser T. Probing the mechanism of exocytosis at the hair cell ribbon synapse. *J Neurosci.* 2007; 27:12933–12944. [PubMed: 18032667]
- Neher E, Sakaba T. Combining deconvolution and noise analysis for the estimation of transmitter release rates at the calyx of held. *J Neurosci.* 2001; 21:444–461. [PubMed: 11160425]
- Nielsen TA, DiGregorio DA, Silver RA. Modulation of glutamate mobility reveals the mechanism underlying slow-rising AMPAR EPSCs and the diffusion coefficient in the synaptic cleft. *Neuron.* 2004; 42:757–771. [PubMed: 15182716]
- Oesch NW, Diamond JS. Ribbon synapses compute temporal contrast and encode luminance in retinal rod bipolar cells. *Nat Neurosci.* 2011; 14:1555–1561. [PubMed: 22019730]
- Palmer MJ, Hull C, Vigh J, von Gersdorff H. Synaptic cleft acidification and modulation of short-term depression by exocytosed protons in retinal bipolar cells. *J Neurosci.* 2003; 23:11332–11341. [PubMed: 14672997]

- Pang JJ, Gao F, Paul DL, Wu SM. Rod, M-cone and M/S-cone inputs to hyperpolarizing bipolar cells in the mouse retina. *J Physiol.* 2012; 590:845–854. [PubMed: 22219344]
- Patneau DK, Vyklicky L Jr, Mayer ML. Hippocampal neurons exhibit cyclothiazide-sensitive rapidly desensitizing responses to kainate. *J Neurosci.* 1993; 13:3496–3509. [PubMed: 7688040]
- Puthussery T, Venkataramani S, Gayet-Primo J, Smith RG, Taylor WR. NaV1.1 channels in axon initial segments of bipolar cells augment input to magnocellular visual pathways in the primate retina. *J Neurosci.* 2013; 33:16045–16059. [PubMed: 24107939]
- Rabl K, Cadetti L, Thoreson WB. Kinetics of exocytosis is faster in cones than in rods. *J Neurosci.* 2005; 25:4633–4640. [PubMed: 15872111]
- Rabl K, Cadetti L, Thoreson WB. Paired-pulse depression at photoreceptor synapses. *J Neurosci.* 2006; 26:2555–2563. [PubMed: 16510733]
- Sagdullaev BT, McCall MA, Lukasiewicz PD. Presynaptic inhibition modulates spillover, creating distinct dynamic response ranges of sensory output. *Neuron.* 2006; 50:923–935. [PubMed: 16772173]
- Sampath AP, Rieke F. Selective transmission of single photon responses by saturation at the rod-to-rod bipolar synapse. *Neuron.* 2004; 41:431–443. [PubMed: 14766181]
- Saszik S, DeVries SH. A mammalian retinal bipolar cell uses both graded changes in membrane voltage and all-or-nothing Na⁺ spikes to encode light. *J Neurosci.* 2012; 32:297–307. [PubMed: 22219291]
- Sheng Z, Choi SY, Dharia A, Li J, Sterling P, Kramer RH. Synaptic Ca²⁺ in darkness is lower in rods than cones, causing slower tonic release of vesicles. *J Neurosci.* 2007; 27:5033–5042. [PubMed: 17494689]
- Singer JH, Diamond JS. Sustained Ca²⁺ entry elicits transient postsynaptic currents at a retinal ribbon synapse. *J Neurosci.* 2003; 23:10923–10933. [PubMed: 14645488]
- Singer JH, Diamond JS. Vesicle depletion and synaptic depression at a mammalian ribbon synapse. *J Neurophysiol.* 2006; 95:3191–3198. [PubMed: 16452253]
- Smith VC, Pokorny J, Lee BB, Dacey DM. Primate horizontal cell dynamics: an analysis of sensitivity regulation in the outer retina. *J Neurophysiol.* 2001; 85:545–558. [PubMed: 11160492]
- Sterling P, Matthews G. Structure and function of ribbon synapses. *Trends Neurosci.* 2005; 28:20–29. [PubMed: 15626493]
- Stiles, JR.; Bartol, TM. Monte Carlo methods for simulating realistic synaptic microphysiology using MCell. In *Computational Neuroscience: Realistic Modeling for Experimentalists*. De Schutter, E., editor. CRC Press; Boca Raton, USA: 2001. p. 87-127.
- Sun JY, Wu LG. Fast kinetics of exocytosis revealed by simultaneous measurements of presynaptic capacitance and postsynaptic currents at a central synapse. *Neuron.* 2001; 30:171–182. [PubMed: 11343653]
- Tansley, K. *Vision in vertebrates*. Chapman and Hall; London: 1965.
- Tsukamoto Y, Omi N. OFF bipolar cells in macaque retina: type-specific connectivity in the outer and inner synaptic layers. *Front Neuroanat.* 2015; 9:122. [PubMed: 26500507]
- von Gersdorff H, Sakaba T, Berglund K, Tachibana M. Submillisecond kinetics of glutamate release from a sensory synapse. *Neuron.* 1998; 21:1177–1188. [PubMed: 9856472]
- Wadiche JI, Jahr CE. Multivesicular release at climbing fiber-Purkinje cell synapses. *Neuron.* 2001; 32:301–313. [PubMed: 11683999]

Bullet points

- Vesicle docking sites at cone ribbons are slowly refilled following release
- Slow vesicle refilling is expected to limit high temporal frequency signaling
- Cones make high gain, readily saturating synapses with cb2 Off bipolar cells
- High gain and saturation hasten synapse recovery to enable high frequency signaling

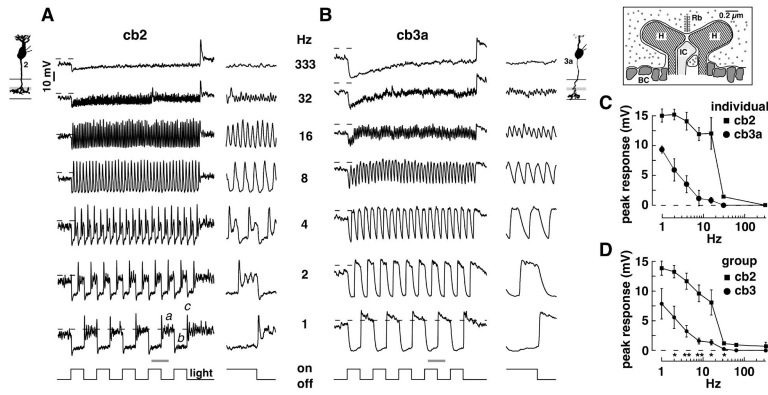


Figure 1. Depolarizing transient amplitude as a function of stimulus frequency in cb2 and cb3 cells

A. Membrane voltage from a cb2 cell was recorded in current clamp during a full-field square wave light stimulus (mean = 1.7×10^6 photons- $\mu\text{m}^{-2}\text{-s}^{-1}$; timing shown below for the 1 Hz trace, frequency is to the right). Baseline voltage, -50.7 mV, is defined as the average voltage during the last 100 ms of the dark phase during the 1 Hz duty cycle (dashed lines). The gray bar shows the location of the expanded responses at right. **B.** Light responses in a cb3a cell with a baseline voltage of -40.8 mV. **C.** Plot of peak response amplitude at light-off relative to baseline versus frequency for the cells in A–B (vertical bars are SEM calculated from all of the light-off transitions at a frequency) and **D.** for all cb2 ($n = 3$) and cb3 ($n = 4$) cells (vertical bars are SEM for the average response of each cell at a frequency). (*) and (**) denote significantly different at $p < 0.05$ and $p < 0.005$, respectively (unpaired t test). *Inset.* Diagram of a cone invagination showing a ribbon (Rb), and the dendritic contacts of horizontal (H), invaginating bipolar (IC), and basal bipolar (BC) cells.

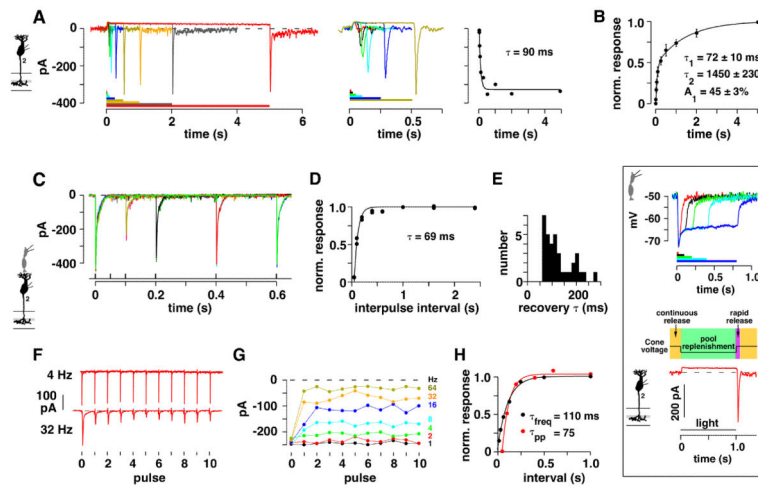


Figure 2. EPSC recovery at the cone to cb2 cell synapse

A. (Left) cb2 cell membrane current during a series of light pulses (4, 25, 50, 100, 250, 500, 1000, 2000, and 5000 ms, shown color-coded below). Stimulus intensity was 1.1×10^6 photons- $\mu\text{m}^{-2}\text{-s}^{-1}$. (Middle) Initial responses on a shorter time scale. (Right) Plot of transient peak amplitude versus light step duration fitted with an exponential curve. **B.** Plot of normalized peak response versus step duration. The responses of individual cells were normalized to their maximum prior to averaging ($n = 8$). Data points were fitted by a double exponential curve. *Inset:* Analogy between a light pulse response and the response during the two pulse paradigm. (Top) Cone voltage responses during light pulses of 25, 100, 200, 400, and 800 ms, shown color-coded below. Responses were uniformly hyperpolarizing. Light intensity = 3.2×10^6 photons- $\mu\text{m}^{-2}\text{-s}^{-1}$. *Inset bottom:* The highly primed vesicle pool is depleted when cones are depolarized in the dark, producing an inward current in a bipolar cell. Replenishment occurs when cones are hyperpolarized during the light step, which corresponds to the interpulse interval. At light-off, cones return to the dark, depolarized level. Ca^{2+} channels open and produce a near synchronous vesicle fusion. **C.** Superimposed cb2 cell responses obtained at different interpulse intervals (two repeats at each interval). A presynaptic cone was depolarized for 1 ms in the loose-seal configuration to a voltage that produced a maximal EPSC response. **D.** Plot of normalized recovery versus interpulse interval from the data shown in 'C' including points from longer intervals not shown. Recovery was fitted with an exponential curve. **E.** Histogram of recovery τ 's ($n = 35$ pairs). **F.** EPSC responses from a different cone to cb2 cell pair during a train of eleven 1 ms depolarizations at 4 and 32 Hz. **G.** Plot of peak response versus pulse number for all stimulus frequencies (1 – 64 Hz; key at right; average of 2 repeats). **H.** Plot of average EPSC peak amplitude for the last eight responses normalized to the first response as a function of interpulse interval (black circles). Paired pulse recovery in the same pair (red circles).

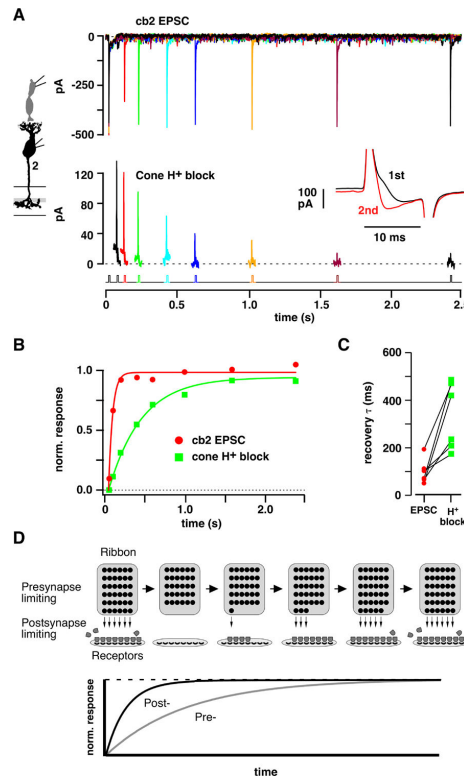


Figure 3. Simultaneous measurement of H⁺ block and cb2 EPSC recovery

A. (Upper panel) Paired pulse response in a cb2 cell during 15 ms cone steps from -70 to -30 mV. (Lower panel) H⁺ block measured as the difference between the current during the first and second steps. With increasing interpulse interval, the H⁺ block during the second pulse more closely approximates that of the first and the difference current becomes smaller. *Inset:* Pair of cone step currents separated by a 50 ms interval. The difference current equals the 1st trace minus the 2nd. **B.** Plot of normalized recovery versus interpulse interval. **C.** Pre- and postsynaptic recovery τ 's. Lines connect simultaneous measurements ($n = 6$ pairs). **D.** Mechanism of fast postsynaptic recovery. After an initial brief depolarization that releases the vesicles docked in the first ribbon row, new vesicles dock and become competent to fuse over time (rightward progression indicated by arrows illustrating the case where the presynaptic recovery is limiting). A second pulse releases the contents (convex shapes) of newly competent vesicles. Postsynaptic recovery can be limiting under conditions where transmitter concentrations are high and receptors saturate before the presynapse fully recovers.

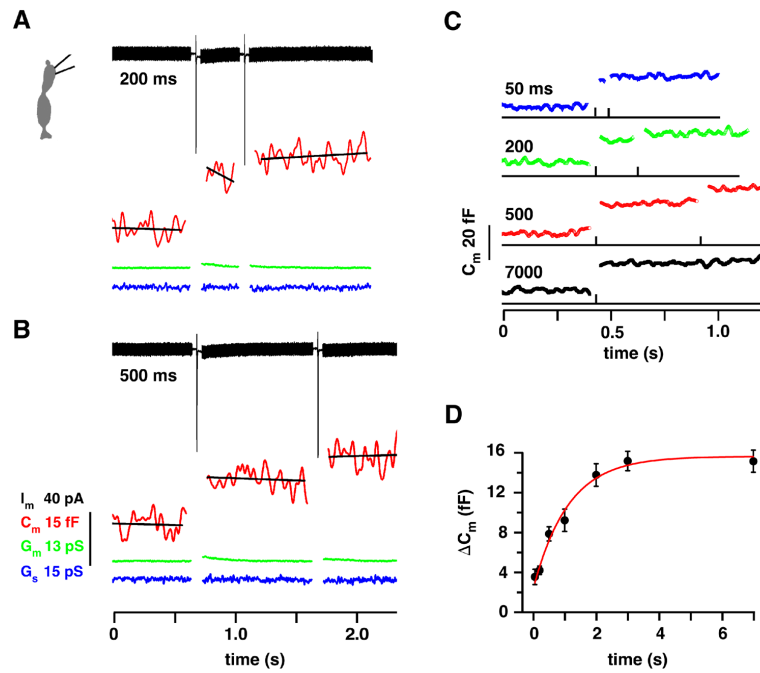


Figure 4. Cone membrane capacitance change (C_m) as a function of interpulse interval

A. C_m was measured before and after 1 ms steps separated by 200 ms. A thick membrane current trace (I_m , black) is produced by the response to the sinusoidal voltage command. The sharp inward deviations result from Ca^{2+} current activation during the 1 ms steps. The Lockin parameters were: membrane conductance (G_m , green trace), C_m (red trace), and series conductance (G_s , blue trace). The capacitance traces were fitted with a straight line to determine the average value. **B.** Same as 'A' but with a 500 ms interval. Steps were from -70 to -10 mV. Scale bars apply to A and B. **C.** Average C_m responses for the interpulse intervals at left ($n = 6$ cones). **D.** Plot of C_m during the second pulse versus interpulse interval. Data was not normalized since the responses to the first jump were similar. The recovery τ was 1.11 s (red curve). Including zero in the fit produced a $\tau = 0.70$ s (not shown).

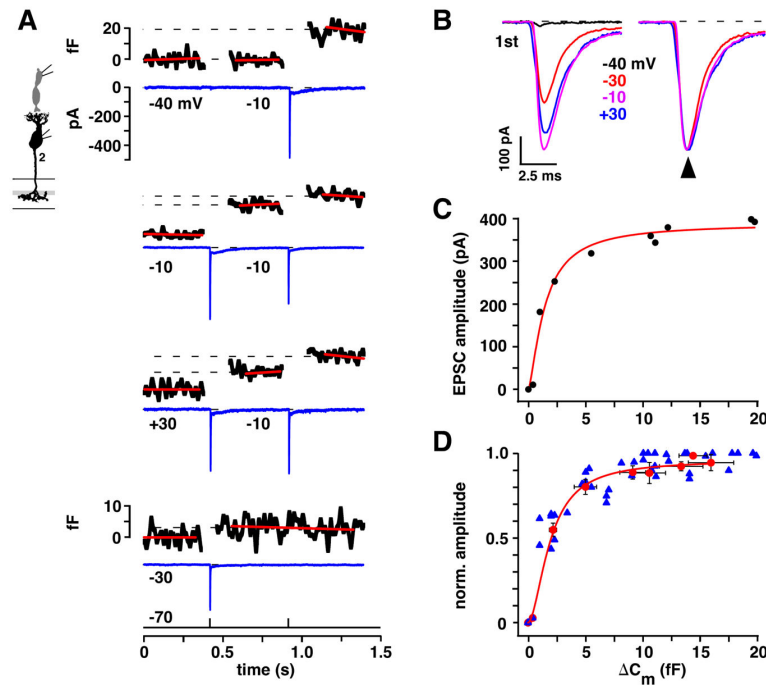


Figure 5. A saturating relationship between cone C_m and cb2 cell EPSC amplitude

A. Responses from a cone to cb2 cell pair. For each set of cone pulses, cone C_m is plotted above and baseline-subtracted cb2 cell current is plotted below. Step voltage (from -70 mV) is indicated below the current trace prior to the corresponding 1 ms pulse. Capacitance and membrane current scales apply throughout except where indicated. The lowermost set of traces contains a single step to -30 mV. **B.** cb2 cell EPSC responses during cone pulses to between -40 and $+30$ mV (left) are shown normalized (right). With the exception of the smallest response, which did not have a corresponding C_m , the responses peaked at the same time (arrow). **C.** Plot of EPSC amplitude versus C_m for the pair in 'A'. EPSC amplitude attained 90% of its maximal value when C_m was ~ 10 fF (Hill fit: $R_{\max} = 388$ pA, $C_{m(1/2)} = 1.44$ fF, $n = 1.42$, $r^2 = 0.97$). **D.** Peak EPSC response is plotted against C_m . Blue triangles show responses during each pulse across all pairs irrespective of pulse voltage. Responses were normalized by the largest EPSC peak amplitude. Red circles replot the data where responses were first normalized to the maximum value in a pair, and then averaged across pairs according to the amplitude of the voltage step, distinguishing between responses obtained during the first and second pulses (Hill fit: $C_{m(1/2)} = 2.3$, $n = 2$, $r^2 = 0.99$). The red curve is fitted to the red circles.

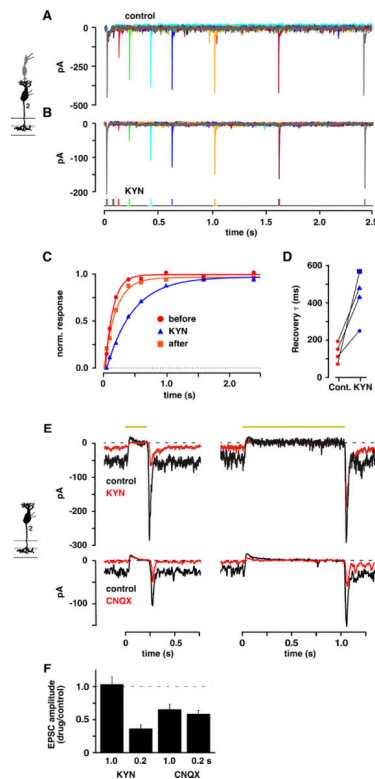


Figure 6. Weak antagonists relieve receptor saturation at the cone to cb2 cell synapse

A cone was depolarized from -70 to -30 mV for 15 ms in whole cell voltage clamp. Paired pulse recovery of the EPSC response was measured in **A**. control and then in **B**. a 2 mM KYN-containing solution. **C**. Normalized recovery versus interpulse interval in control (red circles) and 2 mM KYN (blue triangles). **D**. Recovery τ 's in control and KYN with results from the same pair connected (KYN: blue square = 4 mM; blue circle = 1 mM). The τ in control is an average of before and after treatment. Decreased amplitude (%) in KYN from top to bottom equaled 65.7, 61.3, 58.5, 29.4. **E**. Light responses in control and 1 mM KYN (upper) or 0.4 μ M CNQX (lower) containing-solution during steps of either 0.2 or 1.0 s (light intensity = 3.0×10^6 photons- $\mu\text{m}^{-2}\text{-s}^{-1}$; rows show responses from the same cell; traces are averages). **F**. Histogram of EPSC amplitude in drug (KYN, $n = 6$; CNQX, $n = 9$) divided by control solution for the two light step durations.

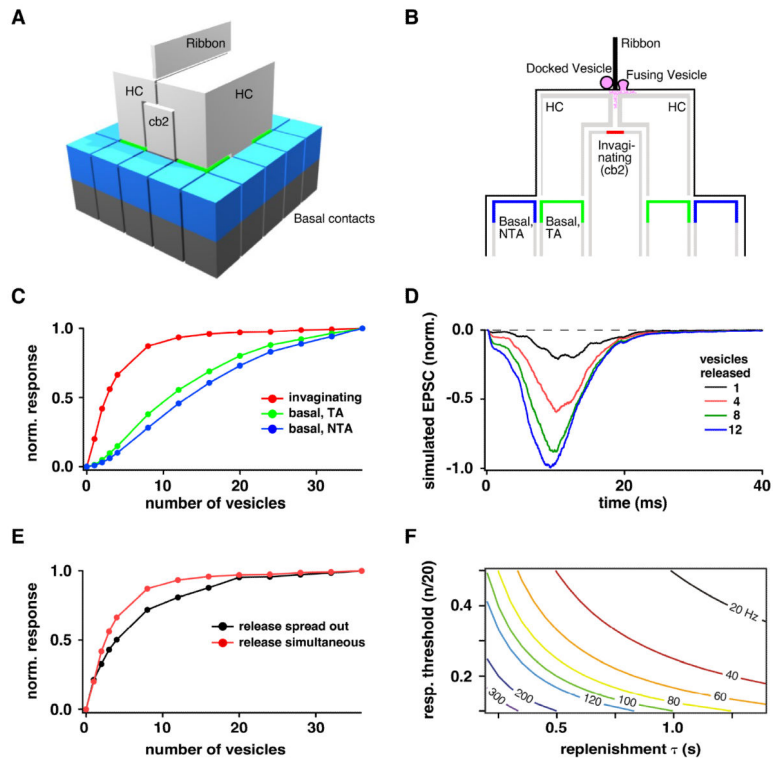


Figure 7. Monte Carlo simulation

A. The model contains a synaptic ribbon, two invaginating horizontal cell (HC) processes, an invaginating bipolar cell process (cb2), and contacts at basal postsynaptic locations (blue and green). The cone membrane is omitted. **B.** A cross-section illustrates the relationship between ribbon docking sites, the synaptic cleft including the cone membrane (thin black line), and the location of postsynaptic receptors, 180 (red) or >500 nm (green and blue) below the release sites. Basal contacts are designated as triad-associated (TA) or non-TA. **C.** Normalized EPSC amplitude versus number of released vesicles for the three different contact locations during synchronous release. **D.** Simulated EPSCs incorporating release jitter. The 20 – 80% rise time of the 12 vesicle response was 4.25 ms. For comparison, the rise time of the transient current response at light-off following a long step is 6.86 ± 0.33 ms and potentially includes variability in the light response among cones. **E.** Normalized EPSC amplitude versus number of vesicles released for synchronous versus temporally-spread release. **F.** Predicted maximum signaling frequency (numbers on selected plots) as a function of response threshold and vesicle replenishment τ (see Discussion). See Figures S1–5 and supplemental experimental procedures for additional information.